Biomedicine & Pharmacotherapy 190 (2025) 118307

Contents lists available at ScienceDirect

Biomedicine & Pharmacotherapy

journal homepage: www.elsevier.com/locate/biopha

Single-cell transcriptomic and pharmacological studies of onvansertib for small cell lung cancer treatment

Hyeon Do Jeon [a,1], Insung Choi [b,1], Woojeung Song [c], Junyang Jung [a,c,d], Jaejung Park [c], Ja-Eun Kim [a,c,e], Ji Hyun Lee [a,c,f], Dong Keon Yon [a,g], Gi Bbeum Lee [h], Seong Hye Ahn [h], Hwajin Lee [a,c,i,*], Inwha Baek [b,j,**]

[a] Department of Precision Medicine, College of Medicine, Kyung Hee University, Seoul 02447, South Korea
[b] Department of Regulatory Science, Graduate School, Kyung Hee University, Seoul 02447, South Korea
[c] Department of Biomedical Science, Graduation School, Kyung Hee University, Seoul 02447, South Korea
[d] Department of Anatomy and Neurobiology, College of Medicine, Kyung Hee University, Dongdaemun-gu, South Korea
[e] Department of Pharmacology, College of Medicine, Kyung Hee University, Seoul 02447, South Korea
[f] Department of Clinical Pharmacology and Therapeutics, College of Medicine, Kyung Hee University, Dongdaemun-gu, South Korea
[g] Department of Digital Health, College of Medicine, Kyung Hee University, Dongdaemun-gu, South Korea
[h] UPPThera, inc.
[i] Department of Biochemistry and Molecular Biology, College of Medicine, Kyung Hee University, Seoul 02447, South Korea
[j] College of Pharmacy, Kyung Hee University, Seoul 02447, South Korea

ARTICLE INFO

Keywords:
Polo-like kinase 1 inhibitors
Onvansertib
Small cell lung cancer
Single-cell RNA-sequencing
Cancer therapies
Pharmacological profiles

ABSTRACT

Polo-like kinase 1 (PLK1), a serine/threonine protein kinase, plays a crucial role in essential biological processes such as cell division, DNA damage response, and cell death. Since its dysregulation is highly associated with tumor development and progression, PLK1 inhibitors, including onvansertib, have been developed as promising anti-cancer therapeutics. Onvansertib is currently under Phase II investigation to evaluate its safety and efficacy in patients with relapsed small cell lung cancer (SCLC). In this study, the efficacy, tolerability, and toxicity of onvansertib were comprehensively profiled using a large panel of 144 cancer cell lines and mouse models. We identified that SCLC cell lines are highly responsive to onvansertib. SCLC xenograft assays showed that daily oral administration of onvansertib at 60 mg/kg was more effective in tumor regression without inducing significant changes in body weight compared to a treatment cycle of 3 days of administration followed by 4 days of rest over a 3-week experimental period. However, *in vivo* toxicity studies revealed onvansertib-related mortality, clinical signs, and hematological adverse effects at the 60 mg/kg dose. Our findings collectively provide experimental evidence to support combination therapies or toxicity-salvaging low-dose regimens, as reflected in current clinical trials of onvansertib. Additionally, we conducted single-cell RNA-sequencing to elucidate the pharmacological mechanisms of onvansertib in SCLC with unprecedented resolution. Onvansertib impairs a normal cell cycle transition by downregulating the cell division process, leading to G2/M phase arrest. Altogether, this work demonstrates the therapeutic mechanisms and *in vitro* and *in vivo* pharmacological profiles of onvansertib in SCLC.

1. Introduction

Polo-like kinase 1 (PLK1), a serine/threonine kinase, is a key regulator of the cell cycle, mitotic entry, centrosome maturation, spindle assembly, chromosome segregation, and cytokinesis [1]. Dysregulation of PLK1 has been linked to tumorigenesis, as its overexpression has been observed in a variety of cancers, including breast, lung, colorectal, and ovarian malignancies [2]. Elevated PLK1 levels are associated with poor prognosis, increased tumor aggressiveness, and resistance to standard therapies, making it a promising therapeutic target for cancer treatment

* Corresponding author at: Department of Precision Medicine, College of Medicine, Kyung Hee University, Seoul 02447, South Korea.
** Corresponding author at: College of Pharmacy, Kyung Hee University, Seoul 02447, South Korea.
E-mail addresses: hwajin2k@khu.ac.kr (H. Lee), ibaek@khu.ac.kr (I. Baek).
[1] Equal contributions

https://doi.org/10.1016/j.biopha.2025.118307
Received 5 March 2025; Received in revised form 27 June 2025; Accepted 1 July 2025
Available online 8 August 2025

[3]. Due to its pivotal role in cell proliferation and survival, extensive research efforts have been directed towards developing small-molecule inhibitors that target PLK1.

Several early-stage studies focused on developing ATP-competitive small-molecule inhibitors targeting PLK1, including BI 2536 and volasertib [4]. While BI 2536 exhibited strong preclinical efficacy, its clinical development was discontinued due to adverse effects and limited efficacy in patients [5]. Volasertib, a more potent second-generation PLK1 inhibitor, showed promising results in preclinical models and early-stage clinical trials, leading to its evaluation in a phase 3 clinical trial for acute myeloid leukemia (AML) [6]. However, despite initial optimism, the phase 3 trial failed to demonstrate a significant improvement in overall survival compared to standard chemotherapy, resulting in the discontinuation of its development [7]. The failure of volasertib highlighted the challenges of targeting PLK1 in clinical settings, including issues related to drug toxicity, acquired resistance, and the need for improved selectivity. These limitations have spurred interest in developing next-generation PLK1 inhibitors with enhanced specificity and improved oral pharmacokinetic properties.

Onvansertib, a third-generation PLK1 inhibitor, has emerged as a promising alternative with superior kinase selectivity for PLK1. *In vitro* studies have demonstrated its potent inhibition of PLK1 activity, leading to mitotic arrest and apoptosis in a range of cancer cell lines, including those resistant to traditional chemotherapy [8]. *In vivo* preclinical models further supported its efficacy, showing tumor growth suppression in xenograft models of colorectal, pancreatic, and prostate cancers [9]. Several clinical trials have reported on its efficacy and safety. A phase 1b study demonstrated its potential in combination with standard-of-care therapies for AML, showing a tolerable safety profile but less promising antitumor activity [10]. Additionally, in metastatic castration-resistant prostate cancer (mCRPC), a phase II trial investigated onvansertib in combination with abiraterone, demonstrating promising responses in patients with resistance to androgen receptor signaling inhibitors, with a notable percentage achieving disease stabilization [11]. In clinical trials for metastatic colorectal cancer, onvansertib has shown efficacy in overcoming resistance to KRAS inhibitors [12]. These findings, altogether, suggest that onvansertib may offer a viable therapeutic option for cancers driven by PLK1 overexpression, particularly when used in combination with other targeted treatments.

Here, we identified small cell lung cancer (SCLC) as one of the promising indications for onvansertib by assessing cell viability for a total of 144 cancer cell lines following treatment. Various *in vitro* mechanistic studies, single-cell RNA-sequencing (scRNA-seq) study, and *in vivo* efficacy and safety studies reveal that onvansertib can work as an effective anticancer agent for SCLC. In SCLC, onvansertib induces cell cycle arrest, DNA damage, and subsequent apoptosis. Additionally, we observed onvansertib-specific cellular responses characterized by unique G2/M phase-enriched scRNA-seq clusters in SCLC. SCLC xenograft assays demonstrated that daily oral administration of onvansertib at 60 mg/kg effectively promotes tumor regression. However, this does resulted in onvansertib-related mortality. Therefore, onvansertib could be a viable therapeutic option with appropriate dosage optimization to mitigate potential toxicity.

2. Materials and methods

2.1. Cell culture

The 146 cell lines used for the cell viability panel screening and their culture media are listed in Supplementary Data 1. All cell cultures were maintained at 37°C with 5 % CO_2.

2.2. Cell viability assay

To evaluate the cytotoxicity of onvansertib, cancer cell lines were seeded into a 96-well culture plate (0.25–2.5 × 10^4 cells/well) in complete media and cultured at 37 °C in the presence of 5 % CO_2. After 3 days, cells were treated with DMSO or onvansertib in a dose range from 3uM to 0.46 nM (3-fold dilutions, a total of 9 concentration points) for 3 days. Cell viability was measured based on quantitation of ATP in the luciferase reaction using the CellTiter-Glo Luminescent Cell Viability Assay kit (Promega, Catalog # G7570). The luminescent signal generated from the luciferase reaction is proportional to the number of viable cells. The cytotoxic effect was evaluated based on the half-maximal cell growth-inhibitory concentration (IC_{50}). Both relative and absolute IC_{50} values were determined using GraphPad Prism.

2.3. Cell cycle arrest assay

SW1271 cells were seeded into a 60 mm cell culture dish at a density of 1 × 10^4 cells. After 24 h, cells were treated with DMSO or 30 nM onvansertib for 28 h. Cells were collected and fixed in cold 70 % ethanol at 4℃ for overnight. The fixed cells were then resuspended with the phosphate-buffered saline (PBS) solution containing propidium iodide (PI) and RNase A, and filtered using a cell strainer. PI staining was performed at room temperature for 40 min before analyzing the cell cycle by flow cytometry. For the dilution experiment, SW1271 cells were seeded into a 25 T flask at a density of 1 × 10^6 cells in 3 ml of complete media and incubated for 24 h. Cells were treated with onvansertib at a final concentration of 60 nM in 1 ml of complete media for 32 h. The dilution of onvansertib was performed by adding 28 ml of complete media to achieve a 1/8 dilution. The cells were harvested after 12 h.

2.4. Immunofluorescence staining

SW1271 cells were treated with DMSO or 30 nM onvansertib for 40 h. Cells were then fixed with 4 % paraformaldehyde (PFA) and permeabilized with 0.25 % Triton X-100 in PBS. After washing twice with PBS, the cells were blocked with 5 % goat serum or 5 % bovine serum albumin in PBS with Tween 20 (PBST). 53BP1 staining was carried out using the anti-53BP1 antibody (1:50, CST, Catalog # 4937S). This primary antibody was detected by Alexa Fluor 488-labeled goat anti-rabbit immunoglobulin G secondary antibodies. For nuclear staining, 4',6'-diamidino-2-phenylindole (DAPI) was used. Images were acquired using a confocal laser scanning microscope (Carl Zeiss, LSM700) or EVOS M7000 microscope (Thermo Fisher Scientific).

2.5. Assessment of cell apoptosis

SW1271 cells were treated with DMSO, 30 nM onvansertib, or 60 nM onvansertib for 72 h. After cell harvesting, cells were washed twice with PBS and stained with fluorescein isothiocyanate (FITC)-conjugated Annexin V in 1× Annexin V binding buffer for 5 min at room temperature. 7-amino-actinomycin D (7-AAD) was then added, and staining was continued in the dark at room temperature for 10 min. After adding 1× Annexin V binding buffer, the cells were processed using LSR II Flow Cytometer (BD Biosciences, BD LSR II). The data were analyzed with BD FACSDiva software (8.0).

2.6. Single-cell RNA-sequencing library preparation

SW1271 cells were treated with DMSO or 30 nM onvansertib for 32 h. A total of 1.59 × 10^6 cells/ml (DMSO) and 1.09 × 10^6 cells/ml (Onvansertib) were used for generating single-cell RNA-sequencing libraries. The libraries were generated using the Chromium Next GEM Single Cell 3' Reagent Kit v3.1 (dual index) (CG000315) and the Chromium Controller (10x Genomics, Pleasanton, California, USA) following the manufacturer's protocol. Briefly, the Chromium Single Cell 3' v3 system encapsulated single cells in a droplet using a gel bead in emulsion (GEM) approach. The gel beads contained a unique 10x barcode (16 nucleotides) and a unique molecular identifier (UMI) (12 nucleotides). A pool of barcoded, full-length cDNA from poly-adenylated mRNA was

produced in a GEM. The released cDNA molecules were cleaned up using Dynabeads MyOne SILANE (ThermoFisher Scientific, cat# 37002D), followed by cDNA amplification. The total cDNA yield was calculated using the Agilent Bioanalyzer 2100 (Agilent, Santa Clara, California, USA). The 3' expression libraries were constructed by performing fragmentation and adaptor ligation. After sample indexing, the libraries were amplified via PCR. Libraries were sequenced on a NovaSeq6000 sequencer (Illumina, San Diego, California, USA) at an average of 20,000 reads per cell. Sequencing reads contain 28 cycles of Read 1 (16 cycles of 10x barcode and 12 cycles of UMI), 90 cycles of Read 2 (insert), and an i7-i5 dual index (10–10 cycles).

2.7. Single-cell RNA-sequencing data analysis

Paired sequencing reads for single-cell RNA-sequencing libraries were aligned to the human reference genome (GRCh38.p14) using Cell Ranger v.8.0.1. Subsequent analyses, including quality control, normalization, feature selection, data scaling, and dimensional reduction with uniform manifold approximation and projection (UMAP) for visualization and clustering, were performed using Seurat v.5.1 [13]. Transcriptomes were filtered for cells with 200–7000 expressed genes and with a fraction of mitochondrial reads < 5 %. The CellCycleScoring function was used to annotate cell cycle phases based on the gene lists associated with the S and G2/M phases [14]. Multiplets were removed using both DoubletFinder v.2.0.4 [15] and scDblFinder v.1.14.0 [16]. After preprocessing, 12,850 and 13,516 cells remained for DMSO- or onvansertib-treated conditions, respectively. Single-cell gene expression data for each condition were merged and normalized using the LogNormalize method with a scale factor of 10,000. For highly variable genes, a scale factor was set to 6500 using the FindVariableFeatures function. Scaling was performed using all genes as features. To identify cell clusters and visualize the data, the first 10 principal components, which captured 72.68 % of the variance, were used to construct UMAP embeddings. Clusters were identified using the FindNeighbors, FindClusters, RunUMAP functions with the following parameters: dims $= 1{:}10$ and resolution $= 0.4$. This clustering analysis resulted in the detection of 11 clusters. Marker genes for each cell cluster were computed using the FindAllMarkers function, with min.pct set to 0.25 while keeping all other parameters at their default values. Each cluster was compared with all remaining cells using the Wilcoxon Rank Sum test. To identify differentially expressed genes (DEGs) in G2/M phase-dominant clusters, the FindMarkers function was applied with default parameters. Genes were considered to be DEGs and marker genes if they had an adjusted p-value < 0.05 and an averaged log2 fold change $> |1|$. GO term analysis was performed using the clusterProfiler v.4.8.3 [17]. All terms with a Benjamini-Hochberg adjusted p-value less than 0.05 were considered significant. Trajectory analysis was performed using velocity v.0.17.17 [18] and scVelo v.3.3 [19].

2.8. Animal studies

Five-week-old BALB/c nude mice (female, CLEA Inc, Japan) and six-week-old ICR mice (JA BIO) were housed according to the ethical regulations. For *in vivo* toxicity experiments, inhalation anesthesia was administered following the regulations. At the end of the experimental protocols, mice were euthanatized.

2.9. Xenograft assay

Five-week-old BALB/c nude mice (female, CLEA Inc, Japan) were used for SCLC xenograft assays. Three SCLC cell lines, NCI-H69, NCI-H1963, and NCI-H526, were examined. Briefly, SCLC cells were cultured in complete media at 37 °C in the presence of 5 % CO_2. Cells were harvested and mixed with Matrigel (1:1). 1×10^7 NCI-H69 cells in 0.2 ml were subcutaneously injected into the right flank of each mouse using a syringe (1 ml, 26 G 1"). For NCI-H1963 and NCI-H526 cells, 5×10^6 cells in 0.2 ml were injected per mouse. Mice with a tumor volume of approximately 150 ± 30 mm were selected. Two dosing regimens of onvansertib were examined: a 3-day on, 4-day off regimen and daily regimen (QD). For the 3-day on, 4-day off group, a vehicle control, 30 mg/kg onvansertib, or 60 mg/kg onvansertib was orally administered once a day for 3 days followed by 4 days off for 3 weeks. Six mice were tested for each treatment condition. The tumor volume and body weight were measured once every 2–3 days for 3 weeks. For the QD group, a vehicle control or 60 mg/kg onvansertib was orally administered once a day for 3 weeks. Six mice were tested for each treatment condition. The tumor volume and body weight were measured once every 2–3 days for 3 weeks. The in vivo efficacy and tolerability of onvansertib were evaluated by changes in tumor volume and animal body weight, respectively. Statistical analysis was performed by comparison to the vehicle control using SPSS statistics (IBM, version 29.0).

2.10. In vivo toxicity analysis

Six-week-old ICR mice (JA BIO) were used to evaluate the *in vivo* toxicity of onvansertib. A vehicle control, 40, 50, or 60 mg/kg onvansertib was orally administered to mice daily (QD) for 4 weeks. To examine sex-dependent toxicity, both male and female mice were tested. Five mice were tested for each treatment condition. Clinical signs of individual mice, mortality, and body weight were monitored and recorded over the course of the study period. Additionally, relative organ weights were measured for the survived mice after 4 weeks of the study period. For the hematological assessment, whole blood was extracted from mice via the abdominal vena cava using a 1 ml syringe (26 G) under respiratory anesthesia. The whole blood was collected into a collection tube containing ethylenediamine tetraacetic acid (EDTA). Hematological analysis was performed, which included measurements of hemoglobin, mean corpuscular volume (MCV), mean corpuscular hemoglobin concentration (MCHC), and counts of white blood cells, neutrophils, lymphocytes, monocytes, eosinophils, basophils, and red blood cells.

2.11. γ-H2AX western blot

SCLC cells were treated with either DMSO (vehicle control), 30 nM, or 60 nM onvansertib for 40 h. After washing twice with cold Dulbecco's PBS (DPBS), total protein lysates were prepared using ice-cold RIPA buffer (150 mM NaCl, 1 % Triton X-100, 1 % sodium deoxycholate, 0.1 % SDS, 50 mM Tris-HCl pH 7.5, 2 mM EDTA) supplemented with 100× protease inhibitor cocktail (GenDepot) and 100× phosphatase inhibitor cocktail (GenDepot). Protein concentrations were determined using the Pierce™ BCA Protein Assay Kit (Thermo Fisher Scientific). Equal amounts of total protein were separated by 10 % SDS-polyacrylamide electrophoresis and transferred to polyvinylidene difluoride (PVDF) membranes (Amersham). Membranes were blocked for 1 h at room temperature in Tris-buffered saline containing 0.1 % Tween-20 (TBS-T) containing 5 % skim milk (BD Difco™), and then incubated overnight at 4 °C with primary antibody diluted in TBS-T containing 5 % bovine serum albumin. After three washes with TBS-T, membranes were incubated with horseradish peroxidase (HRP)-conjugated secondary antibody diluted in 5 % skim milk in TBS-T for 1 h at room temperature. Following another three washes with TBS-T, Chemiluminescent detection was performed using the SuperSignal™ West Pico PLUS Chemiluminescent Substrate (Thermo Fisher Scientific), and images were captured using the ChemiDoc™ XRS+ Imaging System (Bio-Rad). Band intensities were quantified using ImageJ software. The following primary antibodies were used: anti-phospho histone H2A.X (Ser139) (20E3) rabbit monoclonal antibody (1:1000, Cell Signaling Technology, Catalog # 9718S) and anti-α-tubulin rabbit polyclonal Ab (1:1000, Cell Signaling Technology, Catalog # 2144S), anti-GAPDH (D16H11) rabbit monoclonal Ab (1:2000, Cell Signaling Technology, Catalog # 5174S) as loading controls. Goat anti-rabbit IgG H&L (HRP)

(1:3000, Abcam, Catalog #AB6721) was used as a secondary antibody.

2.12. Statistical analyses

Unless otherwise noted, the data generated from the experiments in this study were analyzed using GraphPad Prism (Version 10., San Diego, CA, USA).

3. Results

3.1. Small cell lung cancer cell lines are highly sensitive to onvansertib

To assess the differential cytotoxic effects of onvansertib across various cancer cell lines, we screened a large panel of 144 cancer cell lines, covering 44 different cancer types, along with 2 normal cell lines as controls (Supplementary Data 1). We measured both absolute and relative IC_{50} values of onvansertib in each cell line (Supplementary Figure 1 and Supplementary Data 1). Among these, 117 cell lines were responsive to onvansertib, with absolute IC_{50} values ranging from 0.01 μM to 2.20 μM, and relative IC_{50} values ranging from 0.01 μM to 0.77 μM. Notably, small cell lung cancer (SCLC) exhibited high sensitivity to onvansertib, as five out of six responsive SCLC cell lines (NCI-H1963, NCI-H82, NCI-H446, NCI-H526, and NCI-H211) ranked in the top 20 % based on both absolute and relative IC_{50} values (Fig. 1). The average absolute IC_{50} value for these five SCLC cell lines is 0.024 μM with a standard deviation (SD) of 0.008, while the average relative IC_{50} value is 0.023 μM (SD = 0.008). Thus, the SCLC cell line was selected as a cancer model for further investigation into both *in vitro* and *in vivo* efficacy and toxicity of onvansertib.

3.2. Onvansertib induces DNA damage, G2/M phase arrest, and apoptosis in vitro

TP53-binding protein 1 (53BP1) recognizes DNA double-strand

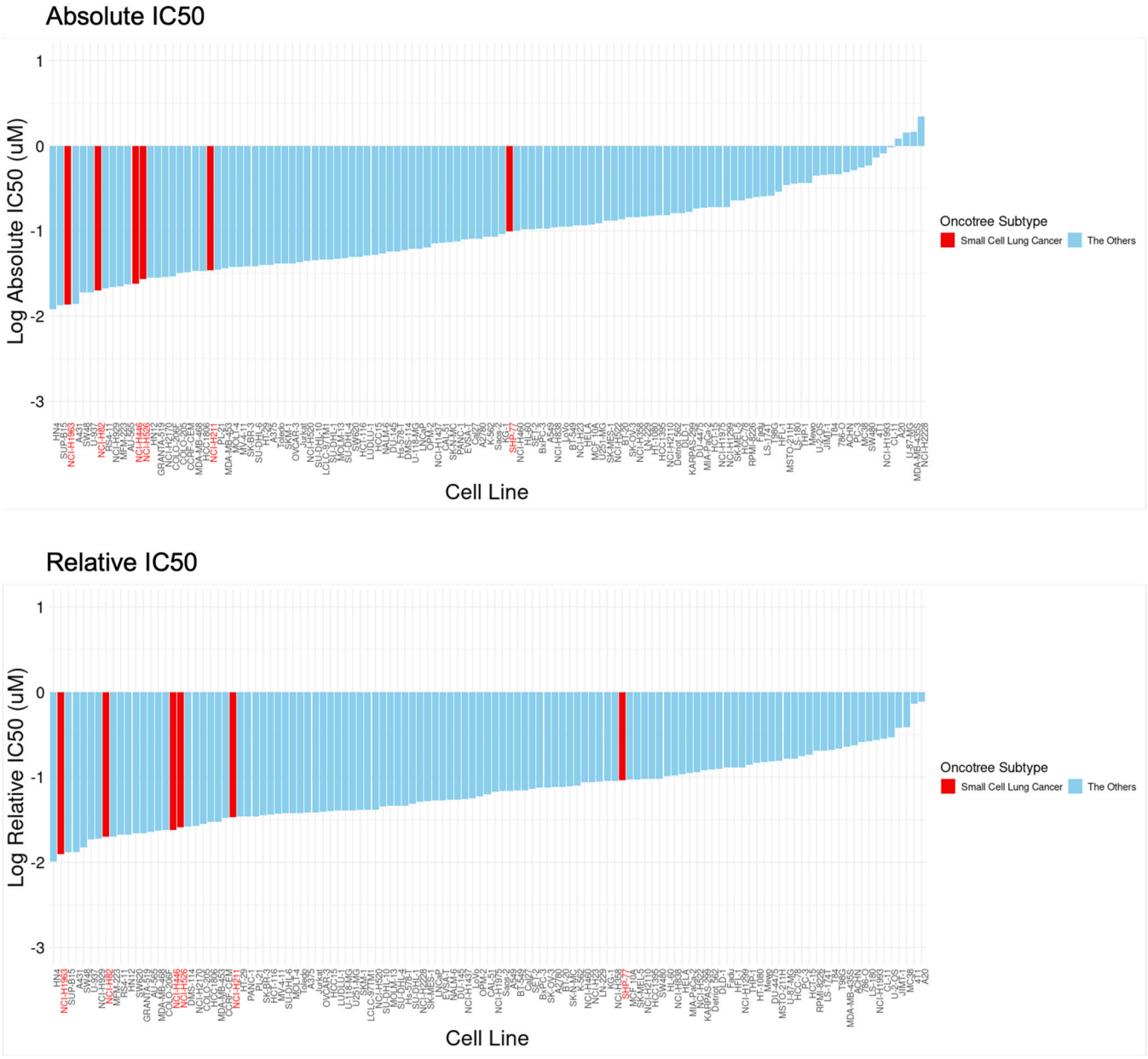

Fig. 1. Cytotoxicity IC_{50} values of onvansertib from the cell viability assay. (A) Log10-transformed absolute IC_{50} values across cancer cell lines. (B) Log10-transformed relative IC_{50} values across cancer cell lines. SCLC cell lines are labeled in red, while all other cell lines are labeled in blue.

break sites and activates the non-homologous end-joining repair pathway [20]. The nuclear localization of 53BP1 is associated with DNA damage and genome instability [21]. To determine whether onvansertib induces DNA damage in the SCLC cell line, we measured 53BP1 nuclear foci in SW1271 and NCI-H526 cells using immunofluorescence staining. A significant increase in the fraction of cells with 53BP1 nuclear foci was observed in both SW1271 and NCI-H526 cells treated with 30 nM onvansertib compared to the DMSO-treated control (Fig. 2A and Supplementary Figure 2). Onvansertib-induced DNA damage was confirmed by assessing γ-H2AX levels in SW1271, NCI-H526, and NCI-H1963 cells. 30 nM onvansertib induced an increase in γ-H2AX levels in NCI-H526 and SW1271, with the highest increase observed in NCI-H526. In contrast, NCI-H1963 cells showed an increase in γ-H2AX levels only at the higher concentration of 60 nM onvansertib (Supplementary Figure 3). Given that PLK1 expression does not correlate with sensitivity to the PLK1 inhibitor volasertib, the differential sensitivity to onvansertib observed across these SCLC lines is more likely attributable to distinct mutational backgrounds [22,23]. The effect of onvansertib on apoptosis was assessed by Annexin V-FITC staining followed by flow cytometry, and apoptotic cells in early and late stages were distinguished by 7-AAD staining (Supplementary Figure 4A). Treatment with 30 nM onvansertib induced apoptosis in approximately 35 % of SW1271 cells, with more than half of the apoptotic cells in the early apoptotic stage (Fig. 2B). The fraction of apoptotic cells increased to approximately 45 % when the concentration of onvansertib was increased to 60 nM (Fig. 2B). Onvansertib-induced apoptosis was further validated in additional SCLC cell lines, including NCI-H526 and NCI-H446 (Supplementary Figure 5A).

To investigate the mechanisms by which onvansertib-induced DNA damage leads to apoptosis, the cell cycle distribution after onvansertib treatment was examined via PI staining-based flow cytometric analysis. Treatment of SW1271 cells with 30 nM onvansertib for 28 h resulted in an increase in cells in the G2/M phase from 19.7 % to 52.2 % with a corresponding decrease in G0/G1 and S phase cells (Fig. 2C and Supplementary Figure 4B). This G2/M phase arrest was more pronounced, with 68.4 % of cells in the G2/M phase when treated with 60 nM onvansertib for 32 h (Fig. 2C and Supplementary Figure 4B). Additionally, to determine if the onvansertib-induced G2/M phase arrest is

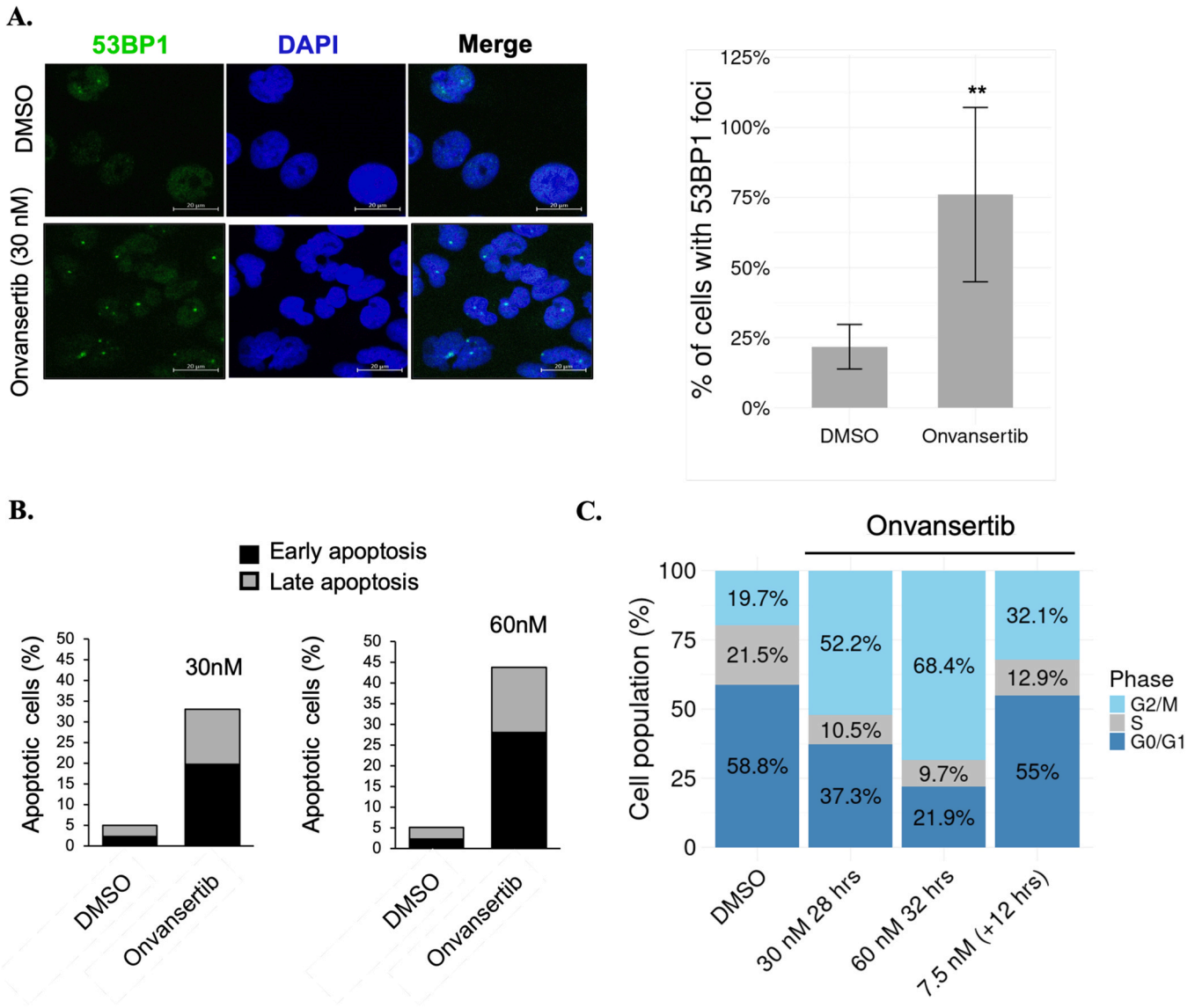

Fig. 2. DNA damage and apoptosis induced by onvansertib. (A) 53BP1 nuclear foci in SW1271 cells treated with 30 nM onvansertib for 40 h. The scale bar represents 20 μm. Data are expressed as mean ± SD. Statistical significance was determined using one-way ANOVA with Tukey's test (**: $P < 0.01$). (B) Percentages of apoptotic SW1271 cells treated with either 30 nM (left) or 60 nM onvansertib (right) for 72 h. (C) Cell cycle distribution in SW1271 cells treated with DMSO, 30 nM, or 60 nM onvansertib. To assess the reversibility of onvansertib-induced G2/M phase arrest, 60 nM onvansertib was diluted to 7.5 nM for an additional 12 h.

reversible, we performed a dilution experiment where onvansertib was diluted 8-fold to a final concentration of 7.5 nM. After 12 h, the proportion of SW1271 cells in the G2/M phase decreased from 68.4 % to 32.1 % (Fig. 2C and Supplementary Figure 4B). Onvansertib-induced G2/M phase arrest was further validated in additional SCLC cell lines, including NCI-H526 and DMS 114 (Supplementary Figure 5B). Taken together, the *in vitro* cytotoxic effect of onvansertib is initiated by DNA damage, which leads to G2/M phase arrest and subsequent apoptosis.

3.3. scRNA-seq identifies cell subpopulations specific to onvansertib treatment

To identify molecular pathways and cell states associated with onvansertib treatment at unprecedented resolution, and to more

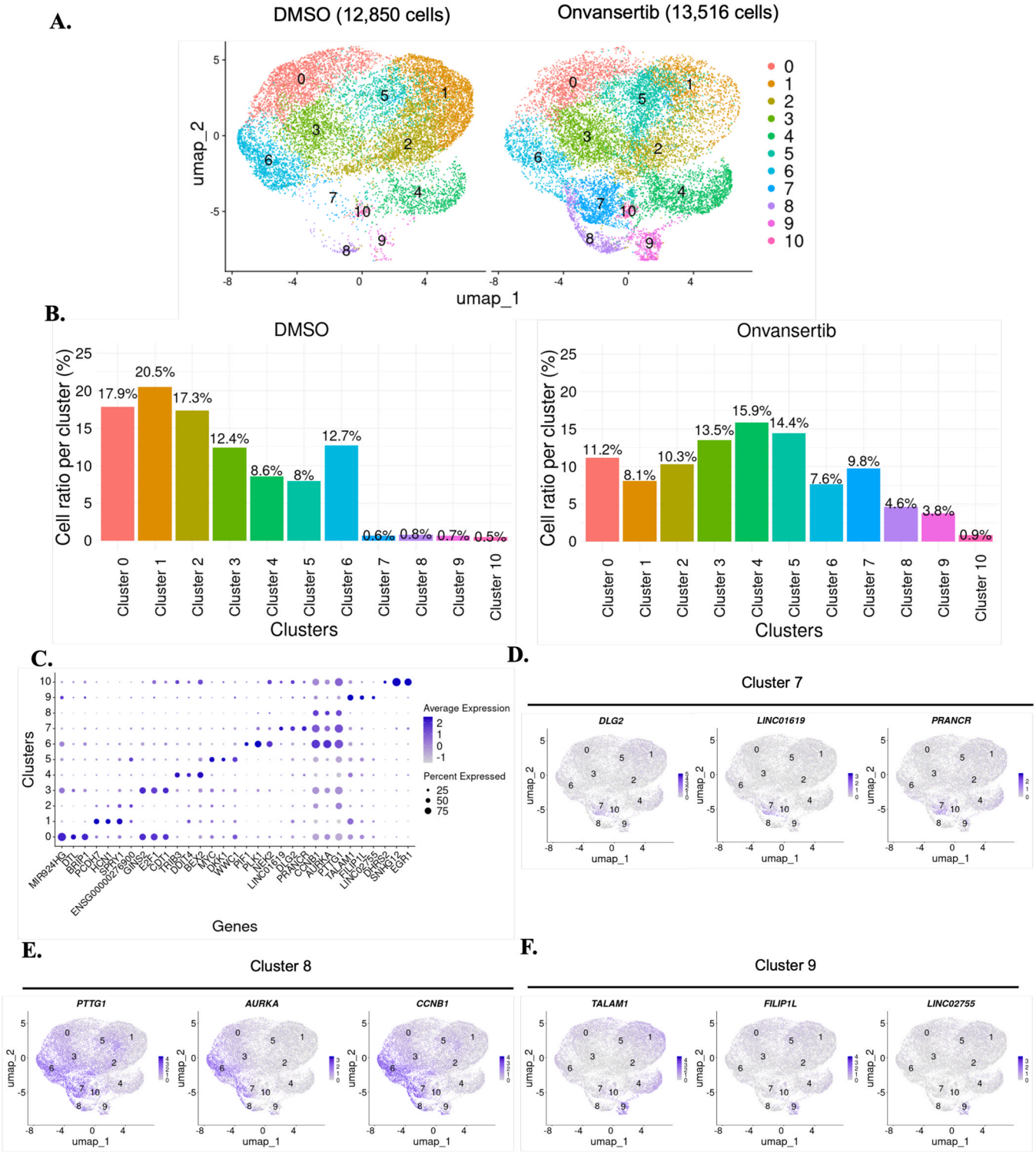

Fig. 3. scRNA-seq based cluster identification of DMSO and onvansertib treated groups. (A) UMAP visualization of merged datasets for DMSO and onvansertib treated (30 nM for 32 h) groups. (B) Cell ratio per cluster in DMSO (12,850 cells) and onvansertib (13,516 cells) groups. (C) Dot plot of marker genes for each cluster, with three markers per cluster except for cluster 2, which has only one marker. (D-F) Feature plots of marker genes for clusters 7, 8, and 9.

precisely monitor the cellular response to onvansertib, we performed scRNA-seq on DMSO- and onvansertib-treated SW1271 cells using the 10x Genomics Chromium system. We observed heterogeneity in gene expression across individual cells, which exhibited continuous patterns, reflecting spectra of cellular states. Dimensionality reduction with UMAP was performed on 12,850 DMSO-treated cells and 13,516 onvansertib-treated cells, resulting in the identification of 11 clusters across both conditions (Fig. 3A). SW1271 cells are known to express *YAP1* [24]. The expression of *YAP1* was confirmed in all clusters (Supplementary Figure 6A). Clusters 7, 8, and 9 were found to be highly specific to the onvansertib treated-condition while other clusters such as cluster 6 were present in both conditions (Fig. 3A and B). Differentially expressed genes and marker genes for each cluster were identified (Fig. 3C and Supplementary Data 2). In Cluster 7, *LINC01619*, *DLG2*, and *PRANCR* were identified as marker genes (Fig. 3D and Supplementary Figure 6B). A low level of *DLG2* expression is associated with cell cycle progression. The long non-coding RNAs (lncRNAs), *LINC01619*, and *PRANCR* are also involved in cell cycle progression. Cluster 8 was characterized by the marker genes *PTTG1*, *AURKA*, and *CCNB1*, which are associated with tumor development (Fig. 3E and Supplementary

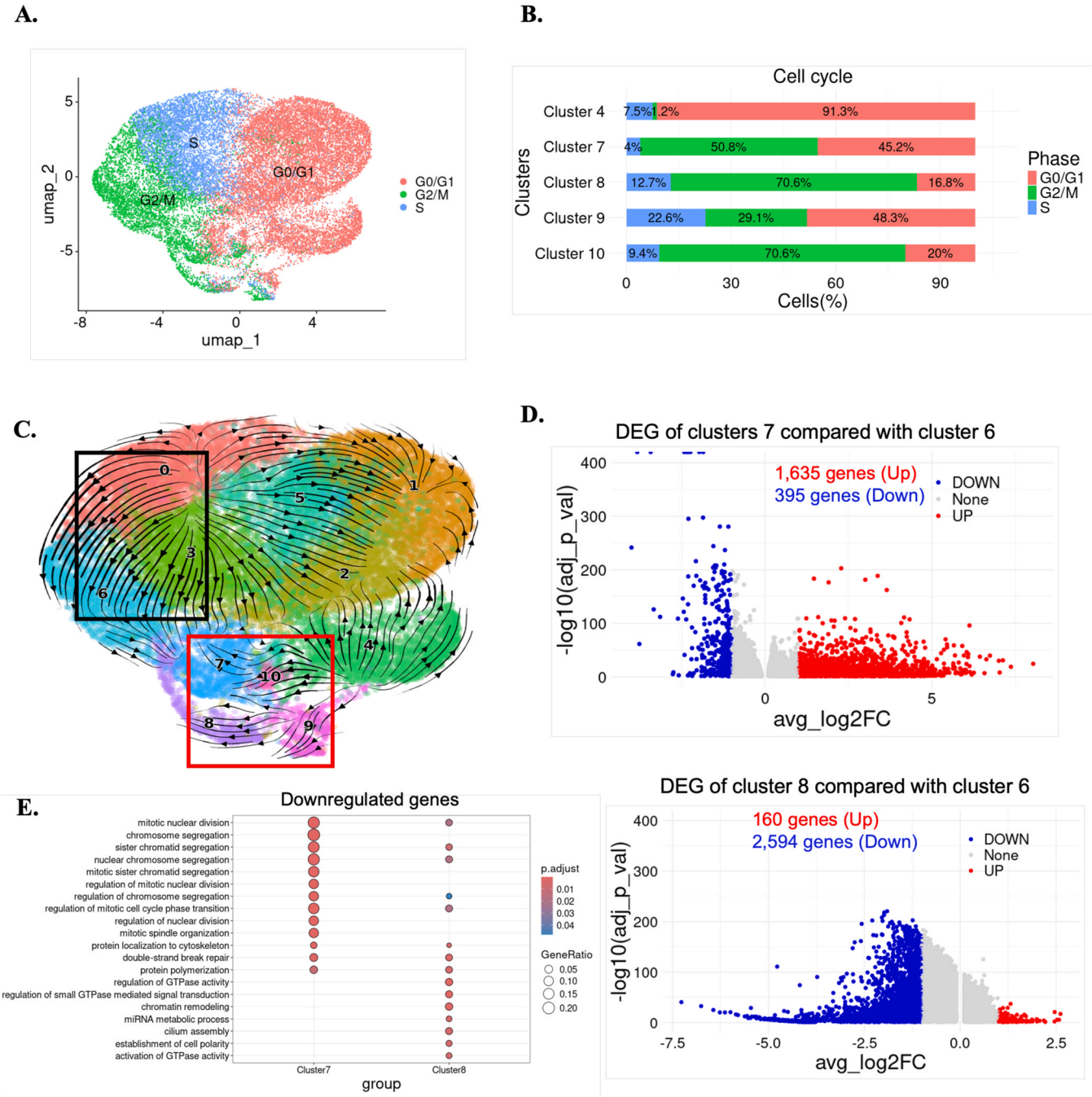

Fig. 4. Profiling of onvansertib-induced transcriptomic changes. (A) UMAP visualization of cell phase classification. (B) Cell cycle phase distribution in onvansertib-enriched clusters. (C) RNA velocity analysis with the black box indicating normal cell cycle transition and the red box indicating onvansertib-induced transition. (D) Volcano plots of differentially expressed genes (DEGs) comparing clusters 7 (top) and 8 (bottom) to cluster 6. Red and blue dots represent upregulated and downregulated DEGs, respectively, while gray dots indicate non-significant changes; DEGs were selected with a log2 fold-change (FC) $> |1|$ and a false discovery rate (FDR) < 0.05. (E) Gene ontology (GO) analysis results for downregulated genes in cluster 7 or 8 compared with cluster 6 (top 10 categories with an FDR threshold < 0.05).

Figure 6C). Cluster 9 cells are marked by *FILIP1L*, *TALAM1*, and *LINC02755* (Fig. 3F and Supplementary Figure 6D). *FILIP1L* inhibits cell proliferation and angiogenesis. The lncRNA *TALAM1* is associated with lung cancer.

3.4. scRNA-seq reveals a distinct onvansertib-induced cell cycle transition

We assessed the cell cycle phases of each cell using cell-cycle scores and projected the inferred cell cycle phases onto a UMAP space (Fig. 4A). The majority of the cells in the clusters specific to onvansertib treatment, namely clusters 7, 8, and 9, were in the G2/M phase, aligning with our *in vitro* findings that onvansertib induces G2/M phase arrest (Fig. 4B and Fig. 2C). Using scVelo, we identified the transcriptional states of each cell, determined the temporal sequence of transcriptional states, and reconstructed the trajectory of cellular states of SW1271 cells. The inferred scVelo trajectory on a UMAP space reveals two distinct directional flows, marked by black and red boxes, respectively (Fig. 4C). The flow in the black box appears to represent a normal cell cycle transition from the S phase (clusters 0 and 3) to the G2/M phase (cluster 6), while the flow in the red box likely represents an abnormal cell cycle transition from the G0/G1 phase (cluster 4) to the G2/M phase (clusters 7, 8, and 10). Given that clusters 7 and 8 are uniquely present in the onvansertib-treated condition, the latter flow might correspond to cells undergoing onvansertib-induced G2/M phase arrest. To investigate the differences in biological and signaling pathways among the G2/M phase-dominant clusters, specifically between clusters 6, 7, and 8, we identified differentially expressed genes. Comparing cluster 7 with cluster 6, we found 1635 upregulated and 395 downregulated genes (FDR < 0.05, $\log_2$-(fold change) $> |1|$) (Fig. 4**D**). When comparing cluster 8 with cluster 6, we identified 160 upregulated and 2594 downregulated genes (FDR < 0.05, $\log_2$-(fold change) $> |1|$) (Fig. 4D). In addition, PLK1 expression was higher in cluster 6, enriched for normal G2/M phase cells, compared to clusters 7 and 8 (Fig. 3C). GO term analyses of the downregulated genes revealed that normal cell division processes, such as mitotic nuclear division, sister chromatid segregation, and nuclear chromosome segregation are significantly downregulated in onvansertib-specific clusters (Fig. 4E). The downregulated genes associated with mitotic nuclear division includes *TTK*, also known as monopolar spindle 1 kinase (*MPS1*). PLK1 is known to cooperate with TTK, primarily by enhancing TTK activity to sustain the spindle assembly checkpoint (SAC) [25]. Our scRNA-seq findings suggest that PLK1 might also regulate TTK expression levels during mitosis. In fact, a dual TTK/PLK1 inhibitor (BAL0891) exhibited potent anticancer activity in triple-negative breast cancer and bladder cancer [26–29]. Interestingly, dual inhibition of TTK and PLK1 resulted in SAC disruption and aberrant mitotic exit, in contrast to the mitotic arrest induced by the TTK-specific inhibitor (CFI-402257) or PLK1-specific inhibitor onvansertib [29]. Moreover, essential biological processes for cellular homeostasis, including GTPase signal transduction, chromatin remodeling, and miRNA metabolic process, are additionally downregulated in cluster 8 (Fig. 4E). Overall, our scRNA-seq results suggest that onvansertib downregulates the cell division process, which impairs cell cycle transition and ultimately leads to G2/M phase arrest.

3.5. Onvansertib inhibits tumor growth in SCLC CDX mouse models

The anti-tumor efficacy of onvansertib was further investigated *in vivo* SCLC cell line-derived xenograft (CDX) mouse models. Since SW1271 cells do not develop solid SCLC tumors in BALB/c nude mice, other SCLC cell lines, including NCI-H69, NCI-H1963, and NCI-H526 were used for xenograft assays. Mice were administered onvansertib orally at different concentrations (30 and 60 mg/kg) or a vehicle control, according to two distinct dosing regimens: 1) once a day for 3 days followed by 4 days off (3-day-on/4-day-off) and 2) daily (QD) (Fig. 5A). Tumor volume and body weight were measured once every 2–3 days over 3 weeks. In the 3-day-on/4-day-off group, tumor volume was reduced by approximately 35 %, while the QD group showed a 91 % reduction in tumor volume in the NCI-H69 xenograft model (Fig. 5B-C). The QD dosing schedule led to tumor regression. Since onvansertib is a reversible PLK1 inhibitor, its effect on PLK1 inhibition seems to be reversed during the 4-day off period. Both onvansertib dosing regimens were tolerated, resulting in weight loss < 10 % (Fig. 5B-C). These results were reproducible with NCI-H1963 and NCI-H526 SCLC CDX mouse models (Fig. 5D-E). Collectively, daily administration is significantly more effective in inhibiting tumor growth than having 4 days off per week without causing notable changes in body weight.

3.6. In vivo toxicity of onvansertib

Daily oral administration of onvansertib (60 mg/kg) effectively inhibited tumor growth in SCLC CDX mouse models. We next evaluated the *in vivo* toxicity of onvansertib in ICR mice by assessing clinical signs, mortality, body weight, and organ weight. Mice were orally administered a vehicle control or onvansertib (40, 50, or 60 mg/kg) daily for four weeks (Fig. 6A). Except for the 40 mg/kg male group, onvansertib-treated mice developed diarrhea and exhibited reduced activity. Furthermore, onvansertib treatment-related mortality was observed in both male and female mice at doses of 50 and 60 mg/kg, 11 days after the initial administration (Fig. 6B). Notably, a dose of 40 mg/kg onvansertib resulted in mortality in female mice as well. For surviving mice, no significant changes in the body weight were observed by the end of the experimental period in both male and female mice (Fig. 6C). In most treatment conditions, the relative organ weights for the lungs, liver, kidneys, and spleen showed no significant differences compared to the vehicle control (Supplementary Figure 7). Lastly, we performed a hematological assessment of onvansertib treatment. A few hematological values, such as the number of red blood cells and lymphocytes and hemoglobin content, were affected by onvensertib administration (Tables 1 and 2).

4. Discussion

Onvansertib is an orally available third-generation PLK1 inhibitor currently undergoing clinical trials for various cancers, including colorectal cancer (NCT06106308) and relapsed SCLC (NCT05450965) [30]. While numerous studies have evaluated the efficacy of onvansertib across different cancer types, comprehensive pharmacological research on its effects in SCLC has not been conducted. This study aims to profile the effects of onvansertib in SCLC for the first time and systematically evaluate its efficacy using both *in vitro* and *in vivo* models. Additionally, scRNA-seq was utilized to elucidate the precise mechanism of onvansertib-induced cell cycle arrest, and an *in vivo* toxicity profiling was conducted to evaluate its clinical applicability. Through these efforts, we aim to contribute foundational knowledge supporting the current and potential clinical applications of onvansertib.

We compared the cytotoxic efficacy of onvansertib across 144 cancer cell lines and confirmed that onvansertib exhibited superior efficacy in SCLC cell lines. We validated that PLK1 inhibition by onvansertib induces DNA damage and genome instability, as demonstrated by the increased 53BP1 foci formation and elevated γ-H2AX expression. Onvansertib treatment led to a substantial accumulation of cells in the G2/M phase, which suggests mitotic arrest. Similar recent findings have been reported in studies investigating other PLK1 inhibitors [31–33]. Notably, the reversibility of G2/M arrest indicates that the cytotoxic effect of onvansertib can be managed by changing dosing strategies at a clinically tolerable range, which may help guide the development of optimized dosing strategies. These results suggest that onvansertib exerts cytotoxicity through a multistep process that begins with PLK1 inhibition and progresses through DNA damage and G2/M arrest before entering apoptosis. scRNA-seq analysis revealed the unique presence of specific clusters in response to the treatment of onvansertib, which were enriched for cells in the G2/M phase. Onvansertib treatment-specific

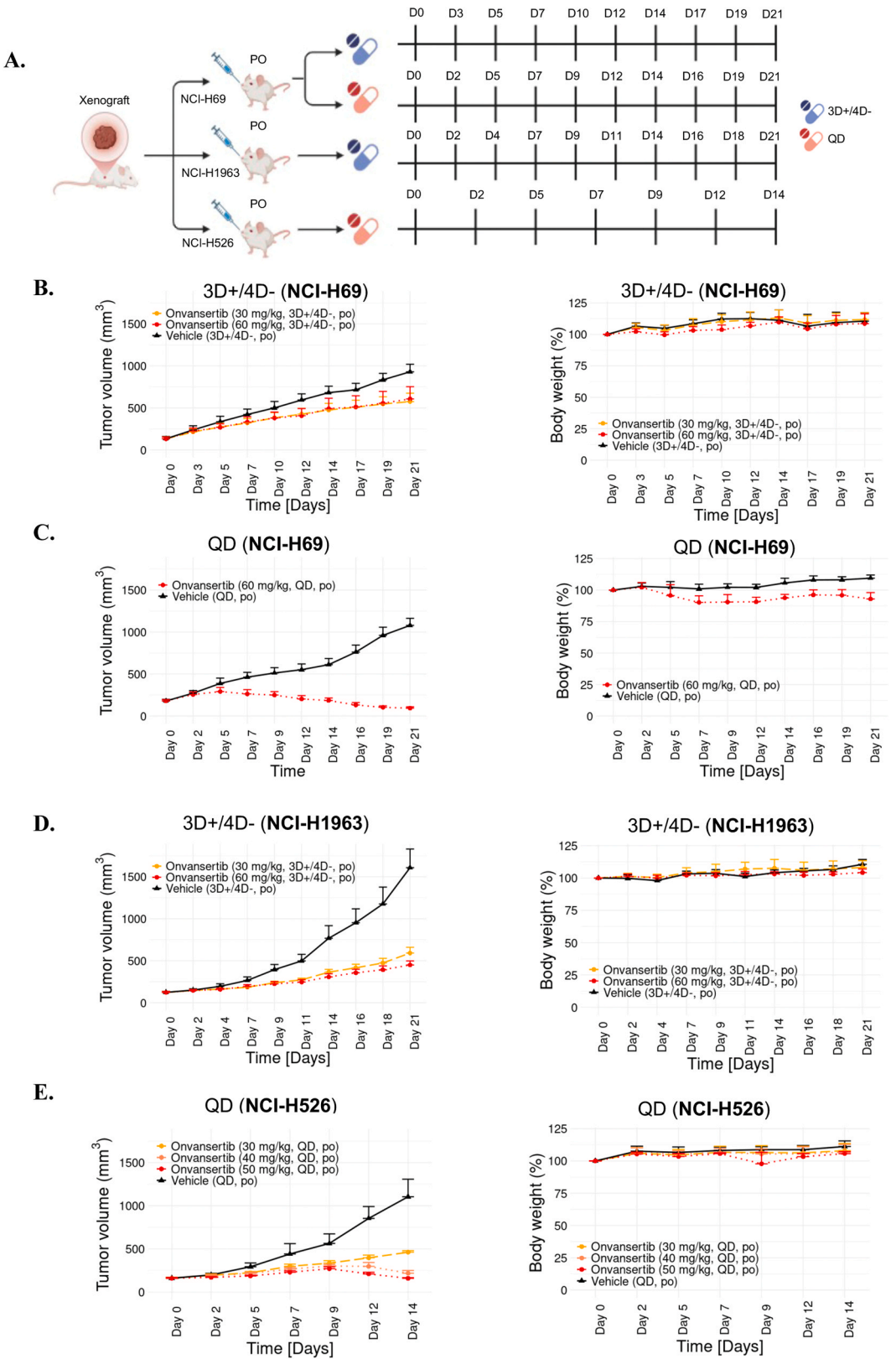

Fig. 5. Anti-tumor efficacy of onvansertib in SCLC CDX (NCI-H69, NCI-H1963 and NCI-H526 cells xenograft) mouse models. (A) Schematic illustration of the experimental design. (B) NCI-H69 xenograft mice treated with the 3D+ /4D- regimen; left: Changes in tumor volume (mm^3) over time, right: Changes in body weight (%) over time ($n = 6$ per group). (C) NCI-H69 xenograft mice treated with the QD regimen; left: Changes in tumor volume (mm^3) over time, right: Changes in body weight (%) over time ($n = 6$ per group). (D) NCI-H1963 xenograft mice treated with the 3D+ /4D- regimen; left: Changes in tumor volume (mm^3) over time, right: Changes in body weight (%) over time ($n = 6$ per group). (E) NCI-H526 xenograft mice treated with the QD regimen; left: Changes in tumor volume (mm^3) over time, right: Changes in body weight (%) over time ($n = 8$ per group). Data are expressed as mean + SD. SCLC: small cell lung cancer, CDX: cell line-derived xenograft, 3D+ /4D-: 3-day-on/4-day-off, QD: quaque die, PO: per oral.

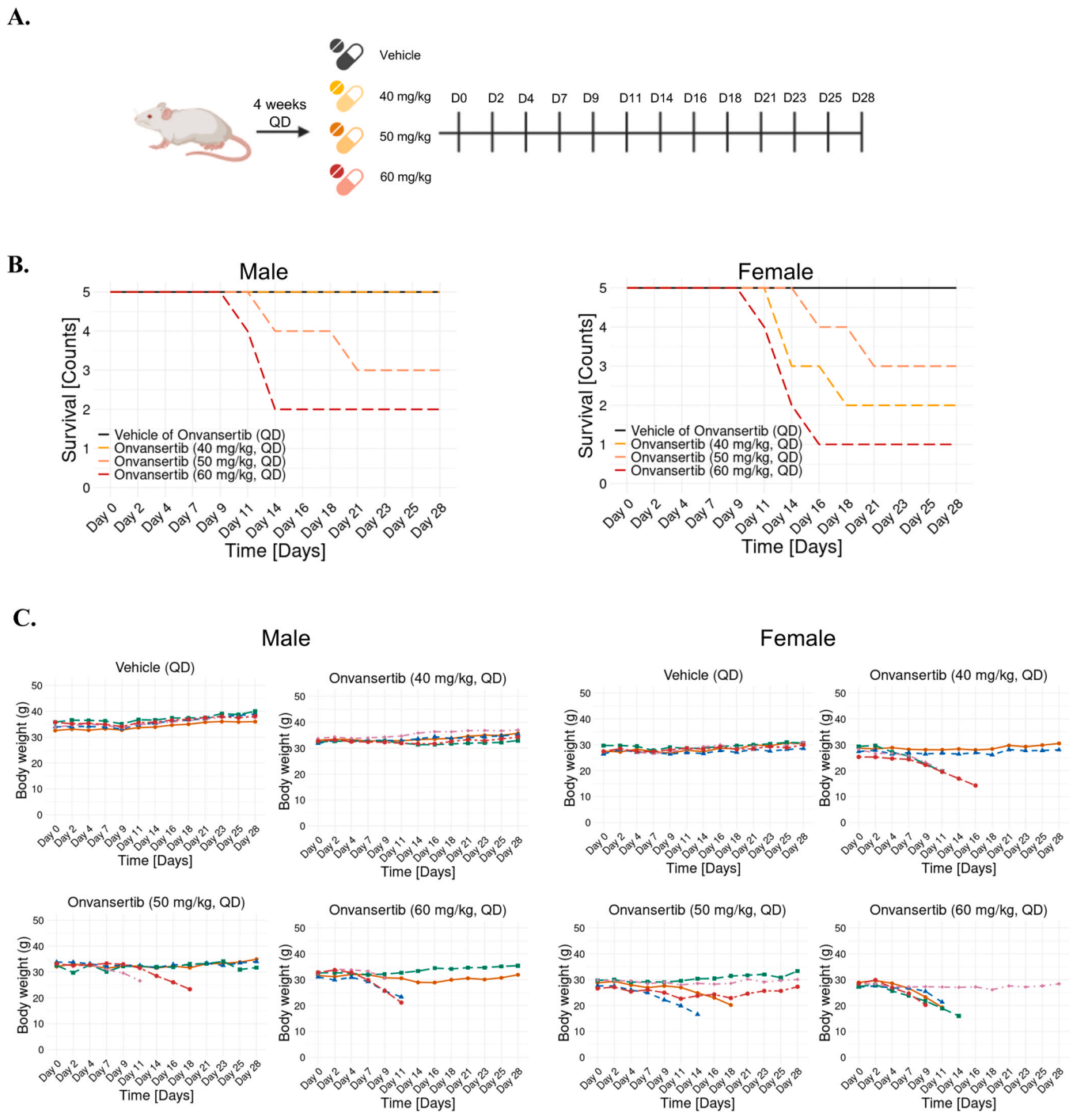

Fig. 6. *In vivo* toxicity of onvansertib in ICR mice. (A) Schematic illustration of the experimental design. (B) Changes in the number of live mice over time; left: male, right: female. (C) Body weight changes in individual mice over time; left: male, right: female. Five mice were examined per condition. Each color corresponds to an individual mouse. Lines missing prior to day 28 indicate death on the day of the last data point.

clusters 7 and 8 showed over a thousand DEGs compared to cluster 6, which represents cells undergoing a normal cell cycle transition. These DEGs are likely downstream effectors of onvansertib and are presumed to collectively mediate onvansertib effect. Importantly, they could serve as a basis for the identification of potential response biomarkers for onvansertib. Future investigation into the association of the DEGs with onvansertib sensitivity would be an interesting direction for future research. GO analysis further indicated that chromosome segregation, a key process in cell cycle progression, was significantly downregulated in clusters 7 and 8. These findings suggest that scRNA-seq can provide insights into the specific mechanisms underlying onvansertib-induced cell cycle arrest, contributing to a more precise understanding of the mechanism of action.

In vivo experiments using xenograft models of various SCLC cell lines showed that the efficacy of onvansertib varied depending on the dosing schedule. The 3-day-on/4-day-off regimen exhibited moderate tumor growth inhibition, whereas the QD 60 mg/kg regimen resulted in tumor regression. Although no onvansertib-related mortality was observed in the *in vivo* efficacy assay using SCLC CDX mouse models, mortality was noted in the *in vivo* toxicity assay conducted in ICR mice even at lower doses (50 mg/kg for male and 40 mg/kg for female). These findings highlight the critical balance between efficacy and toxicity doses when

Table 1
Hematological assessment of onvansertib treatment in male mice.

Parameter	Unit	Vehicle	Onvansertib (QD)		
			40 mg/kg	50 mg/kg	60 mg/kg
RBC	$\times 10^6$/ml	8.49 ± 0.31	6.81 ± 0.67	**5.77 ± 0.41**$^{++}$	**5.38 ± 1.32**$^{++}$
Hemoglobin	g/dL	13.98 ± 0.40	**11.56 ± 1.30**$^{+}$	**10.27 ± 0.55**$^{++}$	**9.8 ± 2.40**$^{++}$
WBC	$\times 10^3$/ml	4.88 ± 2.06	5.8 ± 1.71	4.39 ± 0.61	4.66 ± 2.45
Neutrophils	$\times 10^3$/ml	1.01 ± 0.32	1.94 ± 1.76	1.91 ± 0.91	2.4 ± 2.58
Lymphocytes	$\times 10^3$/ml	3.57 ± 1.68	3.45 ± 0.97	2.09 ± 0.78	1.78 ± 0.16
Monocytes	$\times 10^3$/ml	0.19 ± 0.09	0.24 ± 0.11	0.26 ± 0.05	0.25 ± 0.17
Eosinophils	$\times 10^3$/ml	0.09 ± 0.04	0.14 ± 0.05	0.1 ± 0.02	0.16 ± 0.12
Basophils	$\times 10^3$/ml	0.01 ± 0.01	**0.04 ± 0.01**$^{+}$	0.03 ± 0.01	**0.09 ± 0.02**$^{++}$
Mean corpuscular volume (MCV)	fL	50 ± 0.66	51.16 ± 1.85	**54.07 ± 2.45**$^{+}$	53.5 ± 2.97
Mean corpuscular hemoglobin concentration (MCHC)	g/dL	32.94 ± 0.39	33.12 ± 0.51	32.87 ± 0.80	33.95 ± 1.91

Data are expressed as mean ± SD. One-way ANOVA with Tukey's test ($^{+}$: $P < 0.05$, $^{++}$: $P < 0.01$). Significant changes compared to the vehicle control are highlighted in bold. QD: quaque die.

Table 2
Hematological assessment of onvansertib treatment in female mice.

Parameter	Unit	Vehicle	Onvansertib (QD)		
			40 mg/kg	50 mg/kg	60 mg/kg
RBC	$\times 10^6$/ml	8.63 ± 0.15	7.81 ± 0.19	**6.01 ± 0.67**$^{\#\#}$	6.61
Hemoglobin	g/dL	14.16 ± 0.51	13.4 ± 0.42	**11.17 ± 1.40**$^{\#\#}$	12.2
WBC	$\times 10^3$/ml	4.83 ± 0.50	4.55 ± 2.00	5.07 ± 3.00	3.12
Neutrophils	$\times 10^3$/ml	0.8 ± 0.13	1.21 ± 0.28	1.91 ± 2.14	0.83
Lymphocytes	$\times 10^3$/ml	3.72 ± 0.60	3.07 ± 1.67	2.81 ± 0.76	1.95
Monocytes	$\times 10^3$/ml	0.21 ± 0.15	0.13 ± 0.02	0.21 ± 0.12	0.19
Eosinophils	$\times 10^3$/ml	0.08 ± 0.03	0.12 ± 0.05	0.08 ± 0.01	0.12
Basophils	$\times 10^3$/ml	0.02 ± 0.02	0.03 ± 0.02	0.05 ± 0.03	0.03
Mean corpuscular volume (MCV)	fL	49.22 ± 1.29	51.85 ± 2.90	**55.2 ± 0.95**$^{\#\#}$	55.6
Mean corpuscular hemoglobin concentration (MCHC)	g/dL	33.34 ± 0.13	33.2 ± 0.14	33.57 ± 0.61	33.3

Data are expressed as mean ± SD. One-way ANOVA with Tukey's test ($^{\#}$: $P < 0.05$, $^{\#\#}$: $P < 0.01$). Significant changes compared to the vehicle control are highlighted in bold. QD: quaque die.

using onvansertib as a monotherapy. To the best of our knowledge, this is the first report to characterize the *in vivo* toxicity margin of onvansertib. To overcome this toxicity limitation, combination therapy or a toxicity-salvaging low-dose continuous therapy approach may be necessary. These concepts are already being explored in ongoing clinical trials for colorectal cancer (NCT06106308) and SCLC (NCT05450965) [30]. This study provides foundational data supporting these clinical strategies and contributes to optimizing treatment regimens for onvansertib, ultimately enhancing its clinical applicability.

However, this study has several limitations. First, the xenograft experiments were conducted using mouse models, which limits the direct applicability of the findings to human patients. Therefore, further studies utilizing human-derived samples and the actual clinical results are essential to more clearly validate the effects of onvansertib. Second, the scRNA-seq data used in this study were obtained under a single condition of onvansertib treatment, and validation under various conditions is necessary. Specifically, additional research comparing the effects of onvansertib across different SCLC cell lines or varying drug treatment times and concentrations could provide a more refined mechanistic analysis. Third, this study evaluated the effects of onvansertib as a monotherapy and did not include comparisons with existing treatments or explore combination therapy effects. Therefore, future studies should address these limitations and conduct a more in-depth analysis of onvansertib's effects under various conditions. Based on these findings, the clinical value of onvansertib can be more clearly evaluated, potentially offering more treatment options for SCLC patients and beyond.

In conclusion, this study is expected to contribute to a more objective and comprehensive assessment of onvansertib's therapeutic potential by elucidating its effects and mechanism of action in SCLC.

CRediT authorship contribution statement

Ji Hyun Lee: Resources, Conceptualization. **Junyang Jung:** Resources, Conceptualization. **Woojeung Song:** Methodology, Investigation, Formal analysis, Data curation. **Ja-Eun Kim:** Resources, Conceptualization. **Jaejung Park:** Visualization, Investigation, Formal analysis. **Inwha Baek:** Writing – review & editing, Writing – original draft, Visualization, Supervision, Funding acquisition, Data curation. **Insung Choi:** Writing – review & editing, Visualization, Validation, Investigation, Formal analysis. **Hyeon Do Jeon:** Writing – review & editing, Writing – original draft, Visualization, Software, Methodology, Investigation, Formal analysis, Data curation. **Gi Bbeum Lee:** Supervision, Formal analysis. **Seong Hye Ahn:** Supervision, Formal analysis. **Hwajin Lee:** Writing – review & editing, Writing – original draft, Validation, Supervision, Investigation, Funding acquisition, Formal analysis, Data curation, Conceptualization. **Dong Keon Yon:** Resources, Conceptualization.

Declaration of Generative AI and AI-assisted technologies in the writing process

During the preparation of this work the authors used GPT-4 (OpenAI) in order to improve the readability and language of the manuscript. After using this tool, the authors reviewed and edited the content as needed and take full responsibility for the content of the published article.

Funding and acknowledgement

This work was supported by a grant from the National Research Foundation of Korea (NRF) funded by the Korea government (MSIT) (RS-2023-00278378) and a grant from Kyung Hee University in 2023 (KHU-20231181). We thank UPPThera, inc. members (employees consisting of Keum Young Kang, Im Suk Min, Hyun Lim) for the experiment support.

Declaration of Competing Interest

The authors declare the following financial interests/personal relationships which may be considered as potential competing interests: Hwajin Lee reports a relationship with UPPThera, inc that includes: board membership. If there are other authors, they declare that they have no known competing financial interests or personal relationships that could have appeared to influence the work reported in this paper.

Appendix A. Supporting information

Supplementary data associated with this article can be found in the online version at doi:10.1016/j.biopha.2025.118307.

References

[1] M. Chiappa, S. Petrella, G. Damia, M. Broggini, F. Guffanti, F. Ricci, Present and future perspective on PLK1 inhibition in cancer treatment, Front. Oncol. 12 (2022) 903016.

[2] Z. Liu, Q. Sun, X. Wang, PLK1, a potential target for cancer therapy, Transl. Oncol. 10 (1) (2017) 22–32.

[3] L. Pikor, K. Thu, E. Vucic, W. Lam, The detection and implication of genome instability in cancer, Cancer Metastas.. Rev. 32 (2013) 341–352.

[4] R.E.A. Gutteridge, M.A. Ndiaye, X. Liu, N. Ahmad, Plk1 inhibitors in cancer therapy: from laboratory to clinics, Mol. Cancer Ther. 15 (7) (2016) 1427–1435.

[5] K. Mross, C. Dittrich, W.E. Aulitzky, D. Strumberg, J. Schutte, R.M. Schmid, S. Hollerbach, M. Merger, G. Munzert, F. Fleischer, M.E. Scheulen, A randomised phase II trial of the Polo-like kinase inhibitor BI 2536 in chemo-naive patients with unresectable exocrine adenocarcinoma of the pancreas - a study within the Central European Society Anticancer Drug Research (CESAR) collaborative network, Br. J. Cancer 107 (2) (2012) 280–286.

[6] B.T. Gjertsen, P. Schöffski, Discovery and development of the Polo-like kinase inhibitor volasertib in cancer therapy, Leukemia 29 (1) (2015) 11–19.

[7] H. Döhner, A. Symeonidis, D. Deeren, J. Demeter, M.A. Sanz, A. Anagnostopoulos, J. Esteve, W. Fiedler, K. Porkka, H.J. Kim, Adjunctive volasertib in patients with acute myeloid leukemia not eligible for standard induction therapy: a randomized, phase 3 trial, Hemasphere 5 (8) (2021) e617.

[8] B. Valsasina, I. Beria, C. Alli, R. Alzani, N. Avanzi, D. Ballinari, P. Cappella, M. Caruso, A. Casolaro, A. Ciavolella, NMS-P937, an orally available, specific small-molecule polo-like kinase 1 inhibitor with antitumor activity in solid and hematologic malignancies, Mol. Cancer Ther. 11 (4) (2012) 1006–1016.

[9] A. Hagege, D. Ambrosetti, J. Boyer, A. Bozec, J. Doyen, E. Chamorey, X. He, I. Bourget, J. Rousset, E. Saada, The Polo-like kinase 1 inhibitor onvansertib represents a relevant treatment for head and neck squamous cell carcinoma resistant to cisplatin and radiotherapy, Theranostics 11 (19) (2021) 9571.

[10] A.M. Zeidan, M. Ridinger, T.L. Lin, P.S. Becker, G.J. Schiller, P.A. Patel, A.I. Spira, M.L. Tsai, E. Samuëlsz, S.L. Silberman, A phase Ib study of onvansertib, a novel oral PLK1 inhibitor, in combination therapy for patients with relapsed or refractory acute myeloid leukemia, Clin. Cancer Res. 26 (23) (2020) 6132–6140.

[11] D.J. Einstein, A.D. Choudhury, P.J. Saylor, J.C. Patterson, P. Croucher, M. Ridinger, M.G. Erlander, M.B. Yaffe, G. Bubley, A phase 2 study of onvansertib in combination with abiraterone and prednisone in patients with metastatic castration-resistant prostate cancer (mCRPC), American Society, Clin. Oncol. (2022).

[12] D.H. Ahn, A. Barzi, M. Ridinger, E. Samuëlsz, R.A. Subramanian, P.J. Croucher, T. Smeal, F.F. Kabbinavar, H.-J. Lenz, Onvansertib in combination with FOLFIRI and bevacizumab in second-line treatment of KRAS-mutant metastatic colorectal cancer: a phase Ib clinical study, Clin. Cancer Res. 30 (10) (2024) 2039–2047.

[13] Y. Hao, T. Stuart, M.H. Kowalski, S. Choudhary, P. Hoffman, A. Hartman, A. Srivastava, G. Molla, S. Madad, C. Fernandez-Granda, Dictionary learning for integrative, multimodal and scalable single-cell analysis, Nat. Biotechnol. 42 (2) (2024) 293–304.

[14] I. Tirosh, B. Izar, S.M. Prakadan, M.H. Wadsworth, D. Treacy, J.J. Trombetta, A. Rotem, C. Rodman, C. Lian, G. Murphy, Dissecting the multicellular ecosystem of metastatic melanoma by single-cell RNA-seq, Science 352 (6282) (2016) 189–196.

[15] C.S. McGinnis, L.M. Murrow, Z.J. Gartner, DoubletFinder: doublet detection in single-cell RNA sequencing data using artificial nearest neighbors, Cell Syst. 8 (4) (2019) 329–337.

[16] P.-L. Germain, A. Lun, C.G. Meixide, W. Macnair, M.D. Robinson, Doublet identification in single-cell sequencing data using scDblFinder, f1000research 10 (2022) 979.

[17] T. Wu, E. Hu, S. Xu, M. Chen, P. Guo, Z. Dai, T. Feng, L. Zhou, W. Tang, L. Zhan, clusterProfiler 4.0: a universal enrichment tool for interpreting omics data, innovation 2 (3) (2021).

[18] G. La Manno, R. Soldatov, A. Zeisel, E. Braun, H. Hochgerner, V. Petukhov, K. Lidschreiber, M.E. Kastriti, P. Lönnerberg, A. Furlan, RNA velocity of single cells, Nature 560 (7719) (2018) 494–498.

[19] V. Bergen, M. Lange, S. Peidli, F.A. Wolf, F.J. Theis, Generalizing RNA velocity to transient cell states through dynamical modeling, Nat. Biotechnol. 38 (12) (2020) 1408–1414.

[20] S. Panier, S.J. Boulton, Double-strand break repair: 53BP1 comes into focus, Nat. Rev. Mol. Cell Biol. 15 (1) (2014) 7–18.

[21] L. Anderson, C. Henderson, Y. Adachi, Phosphorylation and rapid relocalization of 53BP1 to nuclear foci upon DNA damage, Mol. Cell Biol. 21 (5) (2001) 1719–1729.

[22] M. Shibata, K. Ham, M.O. Hoque, A time for YAP1: tumorigenesis, immunosuppression and targeted therapy, Int. J. Cancer 143 (9) (2018) 2133–2144.

[23] G. Zhang, A. Pannucci, A.A. Ivanov, J. Switchenko, S.-Y. Sun, G.L. Sica, Z. Liu, Y. Huang, J.C. Schmitz, T.K. Owonikoko, Polo-like kinase 1 inhibitors demonstrate in vitro and in vivo efficacy in preclinical models of small cell lung cancer, Cancers 17 (3) (2025) 446.

[24] J. Ng, L. Cai, L. Girard, O.W.J. Prall, N. Rajan, C. Khoo, A. Batrouney, D.J. Byrne, D.K. Boyd, A.J. Kersbergen, M. Christie, J.D. Minna, M.L. Burr, K.D. Sutherland, Molecular and pathologic characterization of YAP1-expressing small cell lung cancer cell lines leads to reclassification as SMARCA4-deficient malignancies, Clin. Cancer Res 30 (9) (2024) 1846–1858.

[25] C. von Schubert, F. Cubizolles, J.M. Bracher, T. Sliedrecht, G.J. Kops, E.A. Nigg, Plk1 and Mps1 cooperatively regulate the spindle assembly checkpoint in human cells, Cell Rep. 12 (1) (2015) 66–78.

[26] H. Lane, E. Zanini, N. Forster-Gross, K. Litherland, F. Bachmann, L. Bury, N. Willemsem-Seegers, J. De Man, D. Vu-Pham, W. Van Riel, 42P BAL0891: a novel, small molecule, dual TTK/PLK1 mitotic checkpoint inhibitor (MCI) with potent single agent activity, Ann. Oncol. 33 (2022) S18–S19.

[27] H.A. Lane, F. Bachmann, E. Zanini, P. McSheehy, K. Litherland, N. Forster-Gross, L. Bury, D. Vu-Pham, J. de Man, W.E. van Riel, BAL0891: a novel dual TTK/PLK1 mitotic checkpoint inhibitor (MCI) that drives aberrant tumor cell division resulting in potent anti-cancer activity, Cancer Research 82(12_Supplement) (2022), 5645–5645.

[28] J.S. Park, J.-e Lee, M.E. Lee, J. Kim, W.S. Jang, J.J. Lee, J.S. Lee, M. Kang, W. S. Ham, The potential anti-cancer activity of dual TTK/PLK1 inhibitor, BAL0891, in bladder cancer, Cancer Res. 84 (6_ement) (2024), 5726–5726.

[29] E. Zanini, N. Forster-Gross, F. Bachmann, A. Brüngger, P. McSheehy, K. Litherland, K. Burger, A.C. Groner, M. Roceri, L. Bury, Dual TTK/PLK1 inhibition has potent anticancer activity in TNBC as monotherapy and in combination, Front. Oncol. 14 (2024) 1447807.

[30] D.H. Ahn, M. Ridinger, T.L. Cannon, L. Mendelsohn, J.S. Starr, J.M. Hubbard, A. Kasi, A. Barzi, E. Samuëlsz, A. Karki, Onvansertib in combination with chemotherapy and bevacizumab in second-line treatment of KRAS-mutant metastatic colorectal cancer: a single-arm, phase II trial, J. Clin. Oncol. 43 (7) (2025) 840–851.

[31] D. Ataseven, Ş. Taştemur, F. Yulak, S. Karabulut, M. Ergul, GSK461364A suppresses proliferation of gastric cancer cells and induces apoptosis, Toxicol. Vitr. 90 (2023) 105610.

[32] M. Chiappa, A. Decio, L. Guarrera, I. Mengoli, A. Karki, D. Yemane, C. Ghilardi, E. Scanziani, S. Canesi, M.C. Barbera, Onvansertib treatment overcomes olaparib resistance in high-grade ovarian carcinomas, Cell Death Dis. 15 (7) (2024) 521.

[33] B. Moolmuang, J. Chaisaingmongkol, P. Singhirunnusorn, M. Ruchirawat, PLK1 inhibition leads to mitotic arrest and triggers apoptosis in cholangiocarcinoma cells, Oncol. Lett. 28 (1) (2024) 316.